Metabolic interplay between *Proteus mirabilis* and *Enterococcus faecalis* facilitates polymicrobial biofilm formation and invasive disease

Authors: Benjamin C. Hunt[1], Vitus Brix[1], Joseph Vath[1], Lauren Beryl Gutterman[1], Steven M. Taddei[1], Brian S. Learman[1], Aimee L. Brauer[1], and Chelsie E. Armbruster[1]

[1]Department of Microbiology and Immunology, Jacobs School of Medicine and Biomedical Sciences, State University of New York at Buffalo, Buffalo, NY

Abstract

Catheter-associated urinary tract infections (CAUTI) account for 40% of all nosocomial infections and can lead to significant life-threatening complications such as bacteremia. Microbial biofilms play an important role in the development and pathogenesis of CAUTI, and these biofilms are often polymicrobial. *Proteus mirabilis* and *Enterococcus faecalis* are two of the most common causes of CAUTI, and they often persistently co-colonize the catheterized urinary tract. We previously demonstrated that co-culture of *E. faecalis* with *P. mirabilis* increased biofilm biomass, antimicrobial resistance, and disease severity. In this study, we uncover the metabolic interplay that drives biofilm enhancement and examine the contribution of this polymicrobial interaction to CAUTI severity. Though compositional and proteomic biofilm analyses, we determined that the increase in biofilm biomass stems from an increase in the protein fraction of the polymicrobial biofilm. We further observed an enrichment in proteins associated with ornithine and arginine metabolism in polymicrobial biofilms compared to single-species biofilms. By testing mutants of *E. faecalis* and *P. mirabilis,* we found that L-ornithine secreted by the *E. faecalis* ArcD antiporter promotes L-arginine biosynthesis in *P. mirabilis* via ArgF, which ultimately fuels production of proteins that facilitate contact-dependent interactions to enhance biofilm biomass. We further demonstrate that ArcD and ArgF are not important for urinary tract colonization by either species when alone, but ornithine/arginine interplay is critical for the increased disease severity that occurs during coinfection. This study provides deeper insight into the polymicrobial interactions occurring during CAUTI and highlights how these interactions can have significant impacts on pathogenesis and bacterial persistence.

Introduction

Urinary tract infections (UTIs) are among the most common infections worldwide and account for approximately 40% of all nosocomial infections in the United States (1–4). UTIs can be classified into two broad categories, uncomplicated and complicated UTI, dependent upon the presence of risk factors, disease severity, and location of infection (1, 3, 5). Uncomplicated UTIs are infections in otherwise healthy patients and typically resolve with antibiotic treatment, whereas complicated UTIs represent infection in patient with additional risk factors for treatment failure, recurrence, morbidity, or mortality, such as the presence of an indwelling urinary catheter (1, 5). Urinary catheterization is a common procedure in healthcare settings, particularly for the elderly, long-term care patients, and critically ill patients (6–10). Catheter insertion facilitates the development of bacterial colonization through a variety of means, including mechanical disruption, induction of inflammation, and by providing an ideal surface for bacterial attachment (11–14). Each day a urinary catheter is in place, there is a compounding 3-8% incidence of bacteriuria (presence of bacteria in the urine), and the majority of patients with long term catheterization (>28 days) will experience at least one symptomatic CAUTI (6, 15–18). The epidemiology of CAUTI also differs from that of uncomplicated UTI; uncomplicated UTIs are most often caused by *Escherichia coli,* while complicated catheter-associated bacteriuria and CAUTI are caused by a more diverse range of pathogens in addition to *E. coli*, including, *Proteus mirabilis, Enterococcus faecalis, Klebsiella spp., Pseudomonas aeruginosa,* and *Staphylococcus* species (5, 19, 22, 23). Catheter-associated bacteriuria and CAUTI are also frequently polymicrobial, which can further complicate treatment efficacy and infection severity (19–21).

Despite its frequency, polymicrobial CAUTI and the complex polymicrobial interactions occurring during disease are not well understood. Our prior work identified *P. mirabilis* and *E. faecalis* as the most common and persistent co-colonization partners in catheterized individuals (10, 19, 31), suggesting that interactions between these species facilitate persistent colonization. *P. mirabilis* is a Gram-negative rod-shaped bacterium that possess numerous virulence factors (urease, biofilm formation, swarming motility) that contribute to the establishment of CAUTI and progression to secondary infections, and is the most common cause of infection-induced urinary stones, catheter encrustation, and blockage (24–26). *E. faecalis* is a Gram-positive, non-motile, and highly resistant bacterium of growing medical concern (28–30). Both species pose serious challenges to effective treatment that are likely compounded by co-colonization. It is therefore critical to understand the interactions between these two species and to identify potential strategies for disrupting co-colonization.

We previously demonstrated that *P. mirabilis* and *E. faecalis* co-localize on catheters and within the bladder during experimental CAUTI, resulting in polymicrobial biofilms with enhanced biomass and antibiotic resistance (10). However, the underlying mechanism of biofilm enhancement was not elucidated. Coinfection with *P. mirabilis* and *E. faecalis* also dramatically increases the incidence of urinary stone formation (urolithiasis) and bacteremia (39), although it is not yet known if the increase in disease severity is related to increased catheter biofilm biomass. In this study, we uncovered the metabolic interplay that drives biofilm enhancement and examined contribution to infection severity. We demonstrate that secretion of L-ornithine via the ArcD arginine/ornithine antiporter drives L-arginine biosynthesis by *P. mirabilis,* ultimately increase the protein content of polymicrobial biofilms and facilitate dissemination from the urinary tract to the bloodstream. Thus, modulating the metabolic interplay between

these species could potentially disrupt polymicrobial biofilm formation, persistent colonization, and risk of progression to severe disease.

Results

***P. mirabilis* and *E. faecalis* polymicrobial biofilms have increased biofilm biomass that is associated with increased protein content.** *P. mirabilis* and *E. faecalis* are frequent and persistent co-colonizers of catheterized patients and under these conditions we hypothesize that polymicrobial biofilm formation plays a substantial role in mediating the persistence of these two organisms. To investigate this hypothesis, we began by looking at single and polymicrobial biofilm formation in TSB-G (Tryptic soy broth supplemented with 1.5% glucose) under stationary conditions in 24- well plates. Biofilm biomass was assessed using crystal violet staining, while bacterial colony forming units (CFUs) were determined via serial dilution and plating on appropriate agar for each organism. *E. faecalis* forms slightly larger single-species biofilms than *P. mirabilis*; however, when grown together, biofilm biomass is significantly enhanced (Figure 1 A), as previously reported (32). We confirmed that the increase in biofilm biomass was not driven by changes in bacterial viability or counts as ~10^8 CFUs of each species were recovered from the single and co-culture biofilms (Figure 1 B). To determine the source of the increased biofilm biomass, we quantified the amount of extracellular DNA (eDNA), total carbohydrate, and total protein content of the biofilm suspension (BS), the cell-associated fraction of the biofilm (CF), and the NaOH-extracted extrapolymeric substance fraction (EPS) from single and polymicrobial biofilms. No significant increases in eDNA or carbohydrates were observed for the polymicrobial biofilm compared to *P. mirabilis* and *E. faecalis* single-species biofilms (Figure 1 C and D). However, the polymicrobial biofilm had a significant increase in the protein content of the biofilm suspension and cell-associated fraction compared to single-species biofilms (Figure 1 E). Thus, biofilm enhancement appears to be driven by a specific increase in protein content stemming from the cell-associated fraction rather than the EPS. The

importance of protein in mediating the enhancement phenotype was confirmed by establishing biofilms in the presence of 50 µg/mL of proteinase K (PK), which had no effect on single-species biofilms but resulted in a significant reduction in biomass of the polymicrobial biofilm (Figure 1F).

Liquid chromatography mass spectrometry analysis of single and polymicrobial biofilms was next used to identify the proteins that are enriched in the polymicrobial biofilms. This analysis revealed significant differences in protein abundances linked to a variety of metabolic pathways and virulence factors in *P. mirabilis* and *E. faecalis* (Table 1 and Supplemental Material). Proteomic analysis highlighted significant changes in metabolic pathways within *P. mirabilis* and *E. faecalis*, with an increase in abundance of multiple proteins related to ornithine and arginine biosynthesis and metabolism. These changes in ornithine and arginine metabolism drew immediate interest in light of previous work by Keogh et al, wherein L-ornithine export from *E. faecalis*, driven by the ArcD L-ornithine/L-arginine antiporter, modulated biofilm formation, siderophore production, and fitness of *E. coli* (33). As detailed in Figure 2, *P. mirabilis* can either directly metabolize L-ornithine to the polyamine putrescine via *speF*, or it can use L-ornithine for L-arginine biosynthesis via *argF*, which can then also be catabolized to putrescine via *speAB*. We therefore focused on uncovering the contribution of this pathway to polymicrobial biofilm enhancement.

Arginine biosynthesis from ornithine is a critical determinant of *P. mirabilis* fitness *in vitro*. Before investigating the importance of arginine/ornithine metabolism in mediating the biofilm enhancement phenotype, we first examined the growth characteristics of an *E. faecalis arcD* mutant as well as *P. mirabilis* mutants *speF* (PMI0307) and *argF* (PMI3457) under relevant

conditions. Disrupting ornithine export had no impact on *E. faecalis* growth or viability as the *arcD* mutant grew similarly to wild-type OG1RF in brain heart infusion broth (BHI), tryptic soy broth supplemented with 1.5% glucose (TSB-G), and pooled human urine (Figure 3 A, B, & C). Ornithine metabolism and arginine biosynthesis by *P. mirabilis* had no impact on growth or viability in rich media, as the *argF* and *speF* mutants grew similarly to wild-type HI4320 in TSB-G and Luria-Bertani broth (LB) (Figure 3 D & E) and displayed similar motility and urease activity (Supplemental Figure 1). In minimal salts media (PMSM), loss of *speF* had no impact but loss of *argF* completely abrogated *P. mirabilis* growth (Figure 3 F). The *argF* mutant growth defect could be fully rescued by supplementation with either L-citrulline or L-arginine but not by L-ornithine or the arginine catabolic products agmatine or putrescine, demonstrating that mutation of *argF* results in L-arginine auxotrophy in *P. mirabilis* (Figure 3 G-I and Supplement 2).

Human urine is considered to be a nutrient-limited medium for bacteria, providing mainly amino acids and small peptides as nutrient sources (34). When grown in pooled human urine, the *speF* mutant grew similarly to wild-type while viability of the *argF* mutant stopped increasing after ~3 hours (Figure 3 J). This corresponds to the timing of a ~50% reduction in the arginine concentration of urine (from ~134 µM to ~60 µM) by wild-type *P. mirabilis* (35), which is notable as a prior study observed that growth of an *E. coli* arginine auxotroph became limited when the concentration of arginine decreased below 60 µM (36, 37). Importantly, growth of *argF* in human urine could again be rescued by supplementation with L-citrulline, much like growth in minimal medium (Figure 3 J).

Subtle fitness defects can often be further magnified when a mutant strain is directly competing against its parental isolate. We therefore conducted co-challenge experiments in

which cultures were inoculated with a 1:1 mixture of each mutant versus wild-type and a competitive index was calculated based on their ratio at the start of the experiment and hourly thereafter. During direct co-challenge with wild-type *P. mirabilis*, fitness of the *argF* mutant was significantly decreased after just 2 hours of growth in urine, likely due to competition for arginine, and this could again be rescued by supplementation with citrulline (Supplemental 3). In contrast, no fitness defects were observed for the *speF* mutant or the *E. faecalis arcD* mutant. Thus, arginine biosynthesis is critical for *P. mirabilis* growth in minimal medium and fitness in human urine but ornithine secretion by *E. faecalis* and ornithine catabolism to putrescine in *P. mirabilis* are dispensable.

L-ornithine secretion by *E. faecalis* facilitates polymicrobial biofilm enhancement via L-arginine biosynthesis in *P. mirabilis.* To investigate the contribution of *E. faecalis* ornithine export and *P. mirabilis* ornithine metabolism to polymicrobial biofilm enhancement, we established single and polymicrobial biofilms utilizing the *speF*, *argF*, and *arcD* mutants and measured biofilm biomass, CFUs, and biofilm protein content. In TSB-G, none of the mutants exhibited differences in single-species biofilm biomass. However, disrupting *E. faecalis arcD* caused a slight decrease in polymicrobial biofilm biomass, and the combined disruption of *E. faecalis arcD* and *P. mirabilis argF* completely abrogated the polymicrobial biofilm enhancement phenotype (Figure 4 A). These differences were again not driven by any alteration of viable CFUs (Supplement 4), indicating a specific alteration in biofilm biomass.

We previously demonstrated that direct cell-cell contact was required for biofilm enhancement, as neither *P. mirabilis* nor *E. faecalis* exhibited altered biofilm biomass when separated by a transwell insert (32). In agreement with this prior observation, supplementation

with excess L-ornithine alone had no impact on the biomass of any single or polymicrobial biofilm (Figure 4 B). In contrast, supplementation with excess L-arginine alone had no impact the biomass of single-species biofilms but was sufficient to promote increased biomass of polymicrobial biofilms and even restored biomass of the *P. mirabilis* Δ*argF* and *E. faecalis* Δ*arcD* polymicrobial biofilm to the same level as that formed by co-culture of the parental isolates (Figure 4 C). The effect of L-arginine appears to be specifically related to arginine levels rather than the metabolism of L-arginine to catabolic products, as supplementation with agmatine had no impact on the biomass of either single-species or polymicrobial biofilms. We further confirmed that the polymicrobial biofilms formed by *P. mirabilis argF* with *E. faecalis arcD* exhibited significantly reduced protein content (Figure 4 E). Thus, L-arginine is a critical mediator of the interactions that promote polymicrobial biofilm formation and increased protein content.

We next sought to explore the contribution of *E. faecalis* ornithine export and *P. mirabilis* arginine biosynthesis and metabolism to polymicrobial biofilm formation in human urine, as this is the most physiologically-relevant medium for urinary tract pathogens. Biomass enhancement was observed when wild-type *P. mirabilis* and *E. faecalis* were co-cultured (Figure 4 F) and was again independent of any potential impact on bacterial viability (Supplemental 4). None of the mutants exhibited biomass defects in single-species biofilms, but disruption of *arcD* and *argF* again abrogated polymicrobial biofilm enhancement (Figure 4 F). Thus, *E. faecalis* L-ornithine export and *P. mirabilis* arginine biosynthesis are critical components of polymicrobial biofilm formation, including under physiologically relevant conditions.

L-ornithine secretion by *E. faecalis* and L-arginine biosynthesis by *P. mirabilis* contribute to enhanced disease severity and dissemination during polymicrobial infection. We previously demonstrated that polymicrobial infection with *E. faecalis* and *P. mirabilis* substantially increases disease severity during experimental CAUTI and we have also previously demonstrated the importance of biofilm formation to bacterial pathogenesis in the context of CAUTI (32, 38, 39). We therefore sought to determine the contribution of *E. faecalis* L-ornithine secretion and *P. mirabilis* arginine biosynthesis to the successful establishment of polymicrobial catheter biofilms as well as promoting dissemination to the kidneys and bloodstream and overall disease severity. To address this hypothesis, we utilized the *E. faecalis arcD* mutant and the *P. mirabilis argF* mutant to examine the specific contribution of ornithine export and arginine biosynthesis to pathogenesis in the well-established murine CAUTI model (35, 40, 41). Female CBA/J mice aged 6-8 weeks were transurethrally inoculated with 10^5 CFUs of either wild type *P. mirabilis*, the *argF* mutant, wild-type *E. faecalis*, the *arcD* mutant, or polymicrobial mixtures, and a 4mm silicone catheter segment was placed in the bladder during inoculation. Mice were euthanized 96 hours post-inoculation and bacterial burden was quantified in the urine, bladder, kidneys, and spleen (Figure 5).

Neither ArgF nor ArcD were important for establishing single-species infection, as the mutants colonized all organs of the urinary tract to a similar level as the wild-type strains (Figure 5 A&B). There were also no differences in infection severity for *arcD* compared to wild-type *E. faecalis*, and the only difference observed for *argF* was a decrease in the number of mice that developed bacteremia (Table 2). However, differences in disease severity became much more apparent in the context of polymicrobial infection. Both species were detected in all coinfected mice by differential plating (Supplement 5), but mice coinfected with the mutant strains

displayed a consistent trend towards decreased CFUs in all organs compared to mice coinfected with the wild-type strains, although the decrease was only statistically significant in the spleen (Figure 5 C). Strikingly, animals coinfected with the mutant strains had significantly fewer indicators of severe disease as compared to mice coinfected with the wild type strains, including kidney discoloration and mottling, kidney hematoma, and bacteremia (Table 2). The decreased incidence of bacteremia is particularly notable, as an increased incidence of bacteremia is one of the hallmarks of *P. mirabilis* and *E. faecalis* coinfection compared to single-species infection (39). Taken together, these data clearly demonstrate that L-ornithine secretion by *E. faecalis* facilitates L-arginine biosynthesis by *P. mirabilis*, the combined action of which alters polymicrobial biofilm formation and infection severity.

Discussion

Bacterial biofilms and the ability of pathogens to form biofilms has long been noted to be vital for pathogenesis and disease progression in a variety of disease contexts throughout the human body, including CAUTI (42–45). Additionally, there has been a growing appreciation for the fact that many diseases and biofilms are polymicrobial environments, where the network of interactions between bacterial species and the host are important determinants of the overall course of disease development (10, 31, 45–48). However, there is still a dearth of studies addressing and disentangling the interactions that contribute to polymicrobial biofilm formation and infection, let alone their contributions to pathogenesis. Previously, we had demonstrated that *E. faecalis* and *P. mirabilis* are frequent co-colonizers in catheterized patient populations and that they co-localize and form unique biofilm communities with enhanced biofilm biomass, persistence, and antibiotic resistance (10). However, the underlying mechanism was yet to be understood.

Herein, we have demonstrated that L-ornithine secretion from *E. faecalis* feeds into L-arginine metabolism of *P. mirabilis*, resulting in a contact-dependent increases in protein content and biofilm biomass compared to single-species biofilms. Not only were we able to demonstrate that this particularly metabolic interaction influences biofilm formation *in vitro*, but we also uncovered an important role for this cross-feeding in mediating disease severity in a mouse model of polymicrobial CAUTI. This study adds to a growing body of work that metabolic cross-feeding may be a common phenomenon in CAUTI. Previously, Keogh et al (2016) demonstrated that L-ornithine secretion from *E. faecalis* was a major influence on *E. coli* siderophore production and biofilm growth under iron-limitation, and persistence in a wound infection model (49). Our work builds upon this observation and underscores the pivotal role that

E. faecalis L-ornithine secretion plays in mediating polymicrobial interactions in multiple disease contexts.

Considering that supplementation with arginine alone augmented polymicrobial biofilm formation while its catabolic product (agmatine) did not, our data strongly clearly indicate that arginine is the key factor mediating biofilm enhancement. However, the specific fate of arginine remains to be determined. *P. mirabilis* may directly utilize the excess L-arginine for assembly of specific proteins that mediate biofilm enhancement. Alternatively, the L-arginine generated by *P. mirabilis* may be acting as nutrient signal within *P. mirabilis* and triggering phenotypic changes that influence biofilm formation, rather than being directly funneled into protein synthesis. It is also entirely possible that the L-arginine generated by *P. mirabilis* is being exported and taken up by *E. faecalis.* If this is the case, *E. faecalis* may be generating the critical proteins for driving biofilm enhancement. Future efforts will be focused on identifying the protein mediators of biofilm enhancement, distinguishing which microbe is responsible for their production, and defining the role of L-arginine in their biosynthesis.

Given that *P. mirabilis* and *E. faecalis* both exhibit intrinsic resistance to a variety of antibiotics and that polymicrobial biofilm formation further exacerbates these concerns, it is important to consider how this work can be used to develop new approaches to either prevent or disrupt the establishment of these biofilms. Our data suggest that targeting ornithine metabolism and arginine biosynthesis may represent a new avenue for exploration, especially as disrupting these pathways also decreases risk of developing severe disease during experimental infection. However, considering that catheter-associated bacteriuria and CAUTI also frequently involve additional co-colonizing species such as *E. coli*, additional investigations are needed to

understand how other co-colonizing pathogens influence biofilm formation, metabolic cross-feeding, and disease progression.

Methods

Bacterial strains. *Proteus mirabilis* strain HI4320 was isolated from the urine of a long-term catheterized patient in a chronic care facility(50). All *P. mirabilis* mutants used in this study were generated by inserting a kanamycin resistance cassette into the gene of interest following the Sigma TargeTron group II intro protocol as previously described (51, 52). The *P. mirabilis* Δ*speF* mutant was previously constructed (26), while the *argF* mutant was specifically generated for this study. Mutants were verified by selection on kanamycin and PCR. The *Enterococcus faecalis* strain used in this study is an oral clinical isolate, OG1RF (53, 54). The *E. faecalis* Δ*arcD* mutant was previously generated via mariner transposon mutagenesis (33, 55, 56).

Bacterial culture conditions. *P. mirabilis* was cultured at 37°C with shaking at 225 RPM in 5 mL of low-salt LB (LSLB) broth (10 g/L tryptone, 5 g/L yeast extract, 0.1g/L NaCl) or on LSLB plates solidified with 1.5% agar. *E. faecalis* was routinely cultured in 5 mL of Brain Heart Infusion (BHI) broth at 37°C with shaking at 225 RPM or on BHI agar plates solidified with 1.5% agar. *P. mirabilis* mutant strains were grown in media supplemented with 50 µg/mL kanamycin, while *E. faecalis* mutant strains were grown with 8 µg/mL chloramphenicol. Both species of bacteria were also grown in Tryptic Soy Broth supplemented with 1.5% glucose (TSB-G) as indicated. *Proteus mirabilis* minimal salts medium (PMSM) was used in experiments requiring defined growth medium (10.5 g/L K_2HPO_4, 4.5 g/L KH_2PO_4, 1 g/L $(NH_4)_2SO_4$, 15 g/L agar, supplemented with 0.002% nicotinic acid, 1 mM $MgSO_4$, and 0.2% glycerol). PMSM was supplemented further with addition of 10 mM L-ornithine, L-arginine, or L-citrulline as indicated. Filter sterilized pooled human urine from at least 20 de-identified female donors was purchased from Cone Bioproducts (Sequin, TX), stored at -80C, and used as

indicated as a physiologically relevant growth medium. For co-challenge experiments, samples were plated on plain LSLB agar (total CFUs), LSLB with kanamycin (*P. mirabilis* mutant strain CFUs), and BHI agar supplemented with 100 µg/ml spectinomycin (*E. faecalis* CFUs).

Crystal violet staining of bacterial biofilms. Overnight cultures of wild-type or mutant bacteria were adjusted to approximately $2x10^7$ CFU/mL, an OD_{600} of 0.02 for *P. mirabilis* and OD_{600} of 0.04 for *E. faecalis*, in either TSB-G or pooled human urine as indicated, and 750 µL was dispensed in triplicate into the wells of tissue culture treated 24-well plates (Falcon 353047). For polymicrobial biofilms, 325 µL of the appropriate *P. mirabilis* and *E. faecalis* strains were added to the well to a final volume of 750 µL. Sterile media was dispensed in triplicate into wells to serve as a blank for the crystal violet staining. Plates were incubated for 24 hours at 37°C in partially sealed bags with a damp paper towel, after which supernatants were gently aspirated and adherent biofilms were washed twice with 1 mL of 1x phosphate buffered saline (PBS), care was taken to not disrupt the biofilm community. Next, 1 mL of 95% ethanol was added to each well and the plate was incubated at room temperature for 15 minutes, after which ethanol was aspirated and the plate was allowed to air dry with the lid off for 60 minutes. Biofilms were then stained with 0.1% crystal violet and incubated at room temperature for 60 minutes, after such time the crystal violet solution was aspirated and biofilms were washed once with 1 mL of deionized water. Stained biofilms were solubilized in 1 mL of 95% ethanol and plates were incubated at room temperature on a plate shaker at 200 RPM for 15 minutes. Using a micropipette tip, the bottom and sides of wells in the plate were scraped to ensure all stained biofilm biomass was fully resuspended. Crystal violet absorbance was then read at 570 nm using

a BioTek Synergy H1 plate reader. Crystal violet absorbance in all figures is expressed relative to absorbance in the *E. faecalis* monoculture biofilm wells.

Determination of bacterial viability of biofilms. Biofilms were established in triplicate in tissue culture treated 24-well plates as described above and incubated for 24 hours at 37°C. Supernatants were removed, biofilms were gently washed with 1mL of sterile 1x PBS, and scraped as described above to resuspend. Suspensions were then serially diluted and plated onto appropriate agar using an EddyJet 2 spiral plater (Neutec Group) for determination of CFUs using a ProtoCOL 3 automated colony counter (Synbiosis).

Growth curves. Overnight cultures of bacteria were adjusted to approximately $2x10^7$ CFU/mL in the various growth media described above. 200 µL of the adjusted bacterial suspension was distributed in at least triplicate wells of a clear 96-well plate and incubated in a BioTek Synergy H1 96-well plate reader at 37°C with continuous double-orbital shaking and a 1°C temperature differential between the top and bottom of the plate to prevent condensation. Bacterial growth was assessed via absorbance (OD_{600}) every 15 minutes for a period of 18 hours. For assessment of CFUs, 5 mL bacterial suspensions were incubated at 37°C with shaking at 225 RPM, aliquots were taken hourly, serially diluted, and plated onto appropriate agar using an EddyJet 2 spiral plater (Neutec Group) for determination of CFUs using a ProtoCOL 3 automated colony counter (Synbiosis).

Biofilm compositional analysis. Biofilms were established as described above in 24-well plates and incubated for 20 hours at 37°C, with the exception that an entire 24-well plate was used for each inoculum. Compositional analysis was performed as previously described for *P. mirabilis* (57). Briefly, supernatants were removed and all wells of the entire 24-well plate were gently resuspended into a total volume of 3 mL of sterile Milli-Q water, an aliquot was removed from this total volume to generate the biofilm suspension fraction (BS). Suspensions were fixed for 1 hour with formaldehyde (37%) by incubating at room temperature with shaking at 200 RPM. 1 M NaOH was then added and samples were incubated for 3 hours at room temperature with shaking at 200 RPM. Samples were then centrifuged (20,000xg) for 1 hour at 4°C. Supernatant containing the soluble extrapolymeric substance (EPS) was removed and placed in a sterile microcentrifuge tube, while the remaining pellet was resuspended in 1 mL Milli-Q water to generate the cell fraction (CF). The EPS was filtered through a 0.22 µm filter and then was transferred to Slide-A-Lyzer dialysis cassette (Thermofisher, Cat# 66380) and placed in beaker containing Milli-Q water. The Milli-Q water was replaced twice after 2 hours, after which the sample was left to dialyze overnight. Samples were removed from the dialysis cassette to generate the EPS fraction (EPS). All samples were stored at -20C until end point analysis. Total eDNA was determined using the PicoGreen assay (Invitrogen, MP07581), total carbohydrate was determined by phenol-sulfuric acid method as described previously, and total protein was determined via Pierce BCA protein assay kit (Thermofisher, Cat# 23250), all following the manufacturer's instructions (57, 58). For comparison of wild-type and mutant polymicrobial biofilm protein content, biofilms were established in 24-well plates and grown for 24 hours at 37°C, after which three wells were scrapped, pooled, and analyzed as described above.

Liquid-chromatography mass spectrometry (LC-MS) analysis of bacterial biofilms. *Protein digestion:* Biofilm suspension fraction (BS) was prepared as described above. After which, a surfactant-aided precipitation/on-pellet digestion method was adopted in the current study for sample preparation (59). In brief, 100 μg protein was aliquoted from each sample and diluted to 1 μg/μL with 1% SDS. Protein was sequentially reduced by 10 mM dithiothreitol (DTT) at 56°C for 30 min and alkylated by 25 mM iodoacetamide (IAM) at 37°C in darkness for 30 min. Both steps were performed with rigorous vortexing in a thermomixer (Eppendorf). A total of 6 volumes of chilled acetone was then added to each sample with constant vortexing, and the mixture was incubated at -20°C for 3 hr. After centrifugation at 20,000 g, 4°C for 30 min, liquid was decanted, and protein pellet was gently washed by 500 μL methanol and air-dried for 1 min. A volume of 80 μL 50 mM pH 8.4 Tris-formic acid (FA) was then added, and samples were sonicated to loosen the protein pellet. A total volume of 20 μL trypsin (Sigma Aldrich, dissolved in 50 mM pH 8.4 Tris-FA) was added for 6-hr digestion at 37°C with rigorous vortexing in a thermomixer. Digestion was terminated by addition of 1 μL FA, and samples were centrifuged at 20,000 g, 4°C for 30 min. Supernatant was carefully transferred to LC vials for analysis.

LC-MS analysis: The LC-MS system consists of a Dionex μLtimate 3000 nano LC system, a Dinex μLtimate 3000 micro LC system with a WPS-3000 autosampler, and a ThermoFisher Orbitrap Fusion Lumos mass spectrometer. A large-inner diameter (i.d.) trapping column (300-um i.d. x 5 mm) was coupled to the nano LC column (75-um i.d. x 65 cm, packed with 2.5-um Xselect CSH C18 material) for high-capacity sample loading, cleanup and delivery. For each sample, 4 μL derived peptide was injected for LC-MS analysis. Mobile phase A and B were 0.1% FA in 2% acetonitrile (ACN) and 0.1% FA in 88% ACN. The 180-min LC gradient profile was: 4% for 3 min, 4–11 for 5 min, 11–32% B for 117 min, 32–50% B for 10 min, 50–

97% B for 5 min, 97% B for 7 min, and then equilibrated to 4% for 27 min. The mass spectrometer was operated under data-dependent acquisition (DDA) mode with a maximal duty cycle of 3 s. MS1 spectra was acquired by Orbitrap (OT) under 120k resolution for ions within the m/z range of 400-1,500. Automatic Gain Control (AGC) and maximal injection time was set at 120% and 50 ms, and dynamic exclusion was set at 45 s, ± 10 ppm. Precursor ions were isolated by quadrupole using a m/z window of 1.2 Th, and were fragmented by high-energy collision dissociation (HCD). MS2 spectra was acquired OT under 15k resolution with a maximal injection time of 50 ms. Detailed LC-MS settings and relevant information are enclosed in a previous publication by Shen et al.(60).

Data processing: LC-MS files were searched against a NCBI protein sequence database containing both *Proteus mirabilis* and *Enterococcus faecalis* protein sequences using Sequest HT embedded in Proteome Discoverer 1.4 (ThermoFisher Scientific). Target-decoy searching approach using a concatenated forward and reverse protein sequence database was employed for global FDR estimation and control. Searching parameters include: 1) Precursor ion mass tolerance: 20 ppm; 2) Product ion mass tolerance: 0.02 Da; 3) Maximal missed cleavages per peptide: 2; 4) Fixed modifications: carbamidomethylation of cysteine; 5) Dynamic modifications: Oxidation of methionine, Acetylation of peptide N-terminals. Peptide filtering, protein inference and grouping, and FDR control were accomplished by Scaffold v5.0.0 (Proteome Software, Inc.) The filtered peptide-spectrum match (PSM) list was exported. Protein quantification was performed using IonStar, an in-house developed MS1 ion current-based quantitative proteomics method (61). Peptide quantitative features were first generated by a two-step procedure encompassing 1) Chromatographic alignment with ChromAlign for inter-run calibration of retention time (RT) shift; ii) Data-independent MS1 feature generation a direct ion-

current extraction (DICE) method, which extracts ion chromatograms for all precursor ions with corresponding MS2 scans in the aligned dataset with a defined m/z-RT window (10 ppm, 1 min). Both steps were accomplished in SIEVE v2.2 (ThermoFisher Scientific). Post-feature generation data processing was accomplished by UHR-IonStar v1.4 (https://github.com/JunQu-Lab/UHRIonStarApp) (62). The filtered PSM list and the quantitative features database were first integrated by MS2 scan number to generate a list of annotated frames with peptide sequence assignment. The annotated frames were then subjected to dataset-wide normalization, principal component-based detection and removal of peptide outliers, and data aggregation to protein level. Protein quantification results were exported and manually curated and processed in Microsoft Excel.

Mouse model of CAUTI. CAUTI studies were performed as previously described (35, 40, 63). In short, the inoculum was prepared by washing overnight cultures in PBS and adjusting to an OD_{600} of 0.2 for *P. mirabilis* and OD_{600} of 0.4 for *E. faecalis* (~$2x10^8$ CFU/mL), then diluting 1:100 to make a final inoculum of $2x10^6$ CFU/mL. Co-challenge inocula were generated by combining a 50:50 mix of each single-species inoculum. Female CBA/J mice aged 6-8 weeks (Jackson Laboratory) were anesthetized with a weight appropriate dose of ketamine/xylazine (80-120mg/kg ketamine and 5-10 mg/kg xylazine) via IP injection, after which mice were inoculated transurethrally with 50 µL of the appropriate inoculum suspension, delivering ~$1x10^5$ CFU/mouse. A 4 mm segment of sterile silicone tubing (0.64 mm O.D., 0.30 mm I.D., Braintree Scientific Inc.) was advanced into the bladder during inoculation and retained there for the duration of the study as done previously (40, 64). After 96 hours, urine was collected, bladders, kidneys, and spleens were harvested and placed into 5 mL Eppendorf tubes containing 1 mL 1x

PBS. Tissues were homogenized using a Bullet Blender 5 Gold (Next Advance, Speed 8, 4 minutes). Bladders were treated to two cycles to ensure full homogenization. Tissue homogenates were serially diluted and plated onto appropriate agar using an EddyJet 2 spiral plater (Neutec Group) for determination of CFUs using a ProtoCOL 3 automated colony counter (Synbiosis).

Statistical analysis. Statistical significance of experimental results for biofilm, CFU, and growth curve data was assessed by two-way analysis of variance (ANOVA) multiple comparisons or one-way ANOVA as indicated in figure legends. For CAUTI model results, CFUs data was assessed by one-way ANOVA of $\log_{10}$ transformed data and chi-square tests were used to analyzed incidences of abnormalities and health events. These analyses were performed using GraphPad Prism, version 9.3 (GraphPad Software) with a 95% confidence interval.

Acknowledgments

The authors would like to thank Dr. Jun Qu and Dr. Shichen Shen of the NYS Center of Excellent in Bioinformatics and Life Sciences. We would also like to thank Dr. Thomas Russo and members of his laboratory for helpful comments and critiques. This work was funded by the National Institute of Diabetes and Digestive and Kidney Diseases under award R01 DK123158 to CEA. The content is solely the responsibility of the authors and does not necessarily represent the official views of the National Institutes of Health.

References:

1. Sabih A, Leslie SW. 2022. Complicated Urinary Tract InfectionsStatPearls. StatPearls Publishing, Treasure Island (FL).

2. Haque M, Sartelli M, McKimm J, Bakar MA. 2018. Health care-associated infections – an overview. Infection and Drug Resistance 11:2321.

3. Bono MJ, Leslie SW, Reygaert WC. 2022. Urinary Tract InfectionStatPearls. StatPearls Publishing, Treasure Island (FL).

4. Tandogdu Z, Wagenlehner FME. 2016. Global epidemiology of urinary tract infections. Current Opinion in Infectious Diseases 29:73–79.

5. Wagenlehner FME, Bjerklund Johansen TE, Cai T, Koves B, Kranz J, Pilatz A, Tandogdu Z. 2020. Epidemiology, definition and treatment of complicated urinary tract infections. 10. Nat Rev Urol 17:586–600.

6. Hooton TM, Bradley SF, Cardenas DD, Colgan R, Geerlings SE, Rice JC, Saint S, Schaeffer AJ, Tambayh PA, Tenke P, Nicolle LE, Infectious Diseases Society of America. 2010. Diagnosis, prevention, and treatment of catheter-associated urinary tract infection in adults: 2009 International Clinical Practice Guidelines from the Infectious Diseases Society of America. Clin Infect Dis 50:625–663.

7. Nicolle LE. 2012. Urinary catheter-associated infections. Infect Dis Clin North Am 26:13–27.

8. Rogers MAM, Mody L, Kaufman SR, Fries BE, McMahon LF, Saint S. 2008. Use of Urinary Collection Devices in Skilled Nursing Facilities in Five States. Journal of the American Geriatrics Society 56:854–861.

9. Crnich CJ, Drinka P. 2012. Medical device-associated infections in the long-term care setting. Infect Dis Clin North Am 26:143–164.

10. Gaston JR, Andersen MJ, Johnson AO, Bair KL, Sullivan CM, Guterman LB, White AN, Brauer AL, Learman BS, Flores-Mireles AL, Armbruster CE. 2020. Enterococcus faecalis Polymicrobial Interactions Facilitate Biofilm Formation, Antibiotic Recalcitrance, and Persistent Colonization of the Catheterized Urinary Tract. Pathogens 9:835.

11. Guiton PS, Hannan TJ, Ford B, Caparon MG, Hultgren SJ. 2013. Enterococcus faecalis Overcomes Foreign Body-Mediated Inflammation To Establish Urinary Tract Infections. 1. Infect Immun 81:329–339.

12. Peychl L, Zalud R. 2008. [Changes in the urinary bladder caused by short-term permanent catheter insertion]. Cas Lek Cesk 147:325–329.

13. Parsons CL. 1982. Prevention of urinary tract infection by the exogenous glycosaminoglycan sodium pentosanpolysulfate. 1. J Urol 127:167–169.

14. Lila ASA, Rajab AAH, Abdallah MH, Rizvi SMD, Moin A, Khafagy E-S, Tabrez S, Hegazy WAH. 2023. Biofilm Lifestyle in Recurrent Urinary Tract Infections. 1. Life 13:148.

15. Nicolle LE. 2014. Catheter-related urinary tract infection: practical management in the elderly. Drugs Aging 31:1–10.

16. Nicolle LE. 2016. Urinary Tract Infections in the Older Adult. Clinics in Geriatric Medicine 32:523–538.

17. Al-Hazmi H. 2015. Role of duration of catheterization and length of hospital stay on the rate of catheter-related hospital-acquired urinary tract infections. Res Rep Urol 7:41–47.

18. Letica-Kriegel AS, Salmasian H, Vawdrey DK, Youngerman BE, Green RA, Furuya EY, Calfee DP, Perotte R. 2019. Identifying the risk factors for catheter-associated urinary tract infections: a large cross-sectional study of six hospitals. BMJ Open 9:e022137.

19. Gaston JR, Johnson AO, Bair KL, White AN, Armbruster CE. Polymicrobial Interactions in the Urinary Tract: Is the Enemy of My Enemy My Friend? Infection and Immunity 89:e00652-20.

20. Armbruster CE, Prenovost K, Mobley HLT, Mody L. 2017. How Often Do Clinically Diagnosed Catheter-associated Urinary Tract Infections in Nursing Homes Meet Standardized Criteria? J Am Geriatr Soc 65:395–401.

21. Warren JW, Tenney JH, Hoopes JM, Muncie HL, Anthony WC. 1982. A prospective microbiologic study of bacteriuria in patients with chronic indwelling urethral catheters. J Infect Dis 146:719–723.

22. Minardi D, d'Anzeo G, Cantoro D, Conti A, Muzzonigro G. 2011. Urinary tract infections in women: etiology and treatment options. Int J Gen Med 4:333–343.

23. Flores-Mireles AL, Walker JN, Caparon M, Hultgren SJ. 2015. Urinary tract infections: epidemiology, mechanisms of infection and treatment options. Nat Rev Microbiol 13:269–284.

24. Armbruster CE, Mobley HLT, Pearson MM. 2018. Pathogenesis of Proteus mirabilis Infection. EcoSal Plus 8:10.1128/ecosalplus.ESP-0009–2017.

25. Armbruster CE, Hodges SA, Smith SN, Alteri CJ, Mobley HLT. 2014. Arginine promotes Proteus mirabilis motility and fitness by contributing to conservation of the proton gradient and proton motive force. 5. Microbiologyopen 3:630–641.

26. Armbruster CE, Hodges SA, Mobley HLT. 2013. Initiation of Swarming Motility by Proteus mirabilis Occurs in Response to Specific Cues Present in Urine and Requires Excess l-Glutamine. 6. J Bacteriol 195:1305–1319.

27. Breitenbucher RB. 1984. Bacterial changes in the urine samples of patients with long-term indwelling catheters. Arch Intern Med 144:1585–1588.

28. Kline KA, Lewis AL. 2016. Gram-Positive Uropathogens, Polymicrobial Urinary Tract Infection, and the Emerging Microbiota of the Urinary Tract. 2. Microbiol Spectr 4:10.1128/microbiolspec.UTI-0012–2012.

29. Vehreschild MJGT, Haverkamp M, Biehl LM, Lemmen S, Fätkenheuer G. 2019. Vancomycin-resistant enterococci (VRE): a reason to isolate? Infection 47:7–11.

30. Raza T, Ullah SR, Mehmood K, Andleeb S. 2018. Vancomycin resistant Enterococci: A brief review. J Pak Med Assoc 68:768–772.

31. Armbruster CE, Smith SN, Johnson AO, DeOrnellas V, Eaton KA, Yep A, Mody L, Wu W, Mobley HLT. 2017. The Pathogenic Potential of Proteus mirabilis Is Enhanced by Other Uropathogens during Polymicrobial Urinary Tract Infection. 2. Infect Immun 85.

32. Gaston JR, Andersen MJ, Johnson AO, Bair KL, Sullivan CM, Guterman LB, White AN, Brauer AL, Learman BS, Flores-Mireles AL, Armbruster CE. 2020. Enterococcus faecalis Polymicrobial Interactions Facilitate Biofilm Formation, Antibiotic Recalcitrance, and Persistent Colonization of the Catheterized Urinary Tract. 10. Pathogens 9.

33. Keogh D, Tay WH, Ho YY, Dale JL, Chen S, Umashankar S, Williams RBH, Chen SL, Dunny GM, Kline KA. 2016. Enterococcal Metabolite Cues Facilitate Interspecies Niche Modulation and Polymicrobial Infection. Cell Host Microbe 20:493–503.

34. Alteri CJ, Mobley HLT. 2012. Escherichia coli Physiology and Metabolism Dictates Adaptation to Diverse Host Microenvironments. Curr Opin Microbiol 15:3–9.

35. Brauer AL, Learman BS, Taddei SM, Deka N, Hunt BC, Armbruster CE. 2022. Preferential catabolism of l- vs d-serine by Proteus mirabilis contributes to pathogenesis and catheter-associated urinary tract infection. Mol Microbiol 118:125–144.

36. Weerasinghe JP, Dong T, Schertzberg MR, Kirchhof MG, Sun Y, Schellhorn HE. 2006. Stationary phase expression of the arginine biosynthetic operon argCBH in Escherichia coli. BMC Microbiology 6:14.

37. Sezonov G, Joseleau-Petit D, D'Ari R. 2007. Escherichia coli Physiology in Luria-Bertani Broth. J Bacteriol 189:8746–8749.

38. White AN, Learman BS, Brauer AL, Armbruster CE. 2021. Catalase Activity is Critical for Proteus mirabilis Biofilm Development, Extracellular Polymeric Substance Composition, and Dissemination during Catheter-Associated Urinary Tract Infection. 10. Infection and Immunity 89:e00177-21.

39. Learman BS, Brauer AL, Eaton KA, Armbruster CE. 2019. A Rare Opportunist, Morganella morganii, Decreases Severity of Polymicrobial Catheter-Associated Urinary Tract Infection. Infect Immun 88:e00691-19.

40. Armbruster CE, Smith SN, Johnson AO, DeOrnellas V, Eaton KA, Yep A, Mody L, Wu W, Mobley HLT. 2017. The Pathogenic Potential of Proteus mirabilis Is Enhanced by Other Uropathogens during Polymicrobial Urinary Tract Infection. 2. Infect Immun 85.

41. Smith SN, Armbruster CE. 2019. Indwelling Urinary Catheter Model of Proteus mirabilis Infection, p. 187–200. *In* Pearson, MM (ed.), Proteus mirabilis: Methods and Protocols. Springer, New York, NY.

42. Flores-Mireles A, Hreha TN, Hunstad DA. 2019. Pathophysiology, Treatment, and Prevention of Catheter-Associated Urinary Tract Infection. 3. Top Spinal Cord Inj Rehabil 25:228–240.

43. Pelling H, Nzakizwanayo J, Milo S, Denham E l., MacFarlane W m., Bock L j., Sutton J m., Jones B v. 2019. Bacterial biofilm formation on indwelling urethral catheters. Letters in Applied Microbiology 68:277–293.

44. Walker JN, Flores-Mireles AL, Lynch AJ, Pinkner C, Caparon MG, Hultgren SJ, Desai A. 2020. High Resolution Imaging Reveals Microbial Biofilms on Patient Urinary Catheters Despite Antibiotic Administration. 9. World J Urol 38:2237–2245.

45. Vestby LK, Grønseth T, Simm R, Nesse LL. 2020. Bacterial Biofilm and its Role in the Pathogenesis of Disease. Antibiotics (Basel) 9:59.

46. Burmølle M, Ren D, Bjarnsholt T, Sørensen SJ. 2014. Interactions in multispecies biofilms: do they actually matter? Trends in Microbiology 22:84–91.

47. Gabrilska RA, Rumbaugh KP. 2015. Biofilm models of polymicrobial infection. Future Microbiol 10:1997–2015.

48. Gaston JR, Johnson AO, Bair KL, White AN, Armbruster CE. 2021. Polymicrobial Interactions in the Urinary Tract: Is the Enemy of My Enemy My Friend? Infection and Immunity 89:e00652-20.

49. Keogh D, Tay WH, Ho YY, Dale JL, Chen S, Umashankar S, Williams RBH, Chen SL, Dunny GM, Kline KA. 2016. Enterococcal Metabolite Cues Facilitate Interspecies Niche Modulation and Polymicrobial Infection. 4. Cell Host Microbe 20:493–503.

50. Mobley HL, Warren JW. 1987. Urease-positive bacteriuria and obstruction of long-term urinary catheters. J Clin Microbiol 25:2216–2217.

51. Pearson MM, Mobley HLT. 2007. The type III secretion system of Proteus mirabilis HI4320 does not contribute to virulence in the mouse model of ascending urinary tract infection. Journal of Medical Microbiology 56:1277–1283.

52. Armbruster CE, Hodges SA, Mobley HLT. 2013. Initiation of Swarming Motility by Proteus mirabilis Occurs in Response to Specific Cues Present in Urine and Requires Excess l-Glutamine. J Bacteriol 195:1305–1319.

53. Gold OG, Jordan HV, van Houte J. 1975. The prevalence of enterococci in the human mouth and their pathogenicity in animal models. Arch Oral Biol 20:473–477.

54. Dunny GM, Brown BL, Clewell DB. 1978. Induced Cell Aggregation and Mating in Streptococcus faecalis: Evidence for a Bacterial Sex Pheromone. Proceedings of the National Academy of Sciences of the United States of America 75:3479–3483.

55. Kristich CJ, Nguyen VT, Le T, Barnes AM, Grindle S, Dunny GM. 2008. Development and use of an efficient system for random mariner transposon mutagenesis to identify novel genetic determinants of biofilm formation in the core Enterococcus faecalis genome. Applied and Environmental Microbiology 74:3377–3386.

56. Dale JL, Beckman KB, Willett JLE, Nilson JL, Palani NP, Baller JA, Hauge A, Gohl DM, Erickson R, Manias DA, Sadowsky MJ, Dunny GM. 2018. Comprehensive Functional Analysis of the Enterococcus faecalis Core Genome Using an Ordered, Sequence-Defined Collection of Insertional Mutations in Strain OG1RF. mSystems 3:e00062-18.

57. White AN, Learman BS, Brauer AL, Armbruster CE. Catalase Activity is Critical for Proteus mirabilis Biofilm Development, Extracellular Polymeric Substance Composition, and Dissemination during Catheter-Associated Urinary Tract Infection. Infect Immun 89:e00177-21.

58. Masuko T, Minami A, Iwasaki N, Majima T, Nishimura S-I, Lee YC. 2005. Carbohydrate analysis by a phenol–sulfuric acid method in microplate format. Analytical Biochemistry 339:69–72.

59. Shen S, An B, Wang X, Hilchey SP, Li J, Cao J, Tian Y, Hu C, Jin L, Ng A, Tu C, Qu M, Zand MS, Qu J. 2018. Surfactant Cocktail-Aided Extraction/Precipitation/On-Pellet Digestion Strategy Enables Efficient and Reproducible Sample Preparation for Large-Scale Quantitative Proteomics. Anal Chem 90:10350–10359.

60. Shen X, Shen S, Li J, Hu Q, Nie L, Tu C, Wang X, Orsburn B, Wang J, Qu J. 2017. An IonStar Experimental Strategy for MS1 Ion Current-Based Quantification Using Ultrahigh-Field Orbitrap: Reproducible, In-Depth, and Accurate Protein Measurement in Large Cohorts. J Proteome Res 16:2445–2456.

61. Shen X, Shen S, Li J, Hu Q, Nie L, Tu C, Wang X, Poulsen DJ, Orsburn BC, Wang J, Qu J. 2018. IonStar enables high-precision, low-missing-data proteomics quantification in large biological cohorts. Proc Natl Acad Sci U S A 115:E4767–E4776.

62. Wang X, Jin L, Hu C, Shen S, Qian S, Ma M, Zhu X, Li F, Wang J, Tian Y, Qu J. 2021. Ultra-High-Resolution IonStar Strategy Enhancing Accuracy and Precision of MS1-Based Proteomics and an Extensive Comparison with State-of-the-Art SWATH-MS in Large-Cohort Quantification. Anal Chem 93:4884–4893.

63. Smith SN, Armbruster CE. 2019. Indwelling Urinary Catheter Model of Proteus mirabilis Infection. Methods Mol Biol 2021:187–200.

64. Guiton PS, Hung CS, Hancock LE, Caparon MG, Hultgren SJ. 2010. Enterococcal Biofilm Formation and Virulence in an Optimized Murine Model of Foreign Body-Associated Urinary Tract Infections. Infect Immun 78:4166–4175.

Table 1. Liquid chromatography mass spectrometry (LC-MS) analysis shows an upregulation of many ornithine and arginine metabolism related genes. LC-MS analysis summary detailing the ratio of proteins within the polymicrobial biofilms compared to single species biofilms. Proteins involved in metabolism that were at least 2-fold increased in polymicrobial biofilms are displayed, and proteins related to ornithine/arginine metabolism are highlighted in red text.

P. mirabilis		E. faecalis	
Protein Name [Species mapping]	**Ratio**	**Protein Name [Species mapping]**	**Ratio**
arginine ABC transporter substrate-binding protein [Enterobacterales]	2.08	Trk family potassium (K+) transporter, membrane protein [Enterococcus faecalis OG1RF]	81.90
ornithine carbamoyltransferase [Proteus]	2.31	carbamoyl-phosphate synthase, large subunit [Enterococcus faecalis OG1RF]	89.25
2OG-Fe dioxygenase family protein [Proteus]	3.51	hypothetical protein OG1RF_11509 [Enterococcus faecalis OG1RF]	89.74
ornithine decarboxylase SpeF [Proteus mirabilis]	4.03	pyruvate phosphate dikinase [Enterococcus faecalis OG1RF]	90.17
argininosuccinate lyase [Proteus]	4.08	methylmalonate-semialdehyde dehydrogenase (acylating) [Enterococcus faecalis OG1RF]	109.13
UDP-N-acetylglucosamine 2-epimerase (non-hydrolyzing) [Proteus]	4.25	YehR like protein [Enterococcus faecalis OG1RF]	118.52
FAD-dependent oxidoreductase [Proteus]	4.78	dihydrolipoyl dehydrogenase [Enterococcus faecalis OG1RF]	132.58
fimbrial chaperone [Proteus]	5.72	anaerobic ribonucleoside-triphosphate reductase large subunit [Enterococcus faecalis OG1RF]	149.40
argininosuccinate synthase [Proteus]	6.18	3-methyl-2-oxobutanoate dehydrogenase [Enterococcus faecalis OG1RF]	154.12
electron transport complex subunit RsxC [Enterobacterales]	7.12	ABC superfamily ATP binding cassette transporter, ABC/membrane protein [Enterococcus faecalis OG1RF]	211.30
nitrogen regulation protein NR(II) [Enterobacterales]	7.29	spermidine/putrescine ABC superfamily ATP binding cassette transporter, ABC protein [Enterococcus faecalis OG1RF]	264.33
ABC transporter permease [Proteus]	7.95	2-dehydropantoate 2-reductase [Enterococcus faecalis OG1RF]	476.32
acetylglutamate kinase [Proteus mirabilis]	8.23	selenium-dependent molybdenum hydroxylase 1 [Enterococcus faecalis OG1RF]	627.14
N-acetyl-gamma-glutamyl-phosphate reductase [Proteus]	10.62	branched-chain alpha-keto acid [Enterococcus faecalis OG1RF]	666.84
hypothetical protein [Proteus]	13.23	putative transcriptional activator SrlM [Enterococcus faecalis OG1RF]	1088.25
LysR family transcriptional regulator [Proteus]	14.92	5-dehydro-2-deoxygluconokinase [Enterococcus faecalis OG1RF]	1487.36

Table 2. Disruption of metabolic cooperation between *E. faecalis* and *P. mirabilis* results in a significant reduction in disease severity and tissue invasion in polymicrobial CAUTI infection. Incidence of bacteremia and tissue abnormalities in murine CAUTI infections. Chi-square test used to determine if frequency of events were statistically different between groups.

Adverse health event or tissue abnormality	**Pm**	**ΔargF**	**P value**	**Ef**	**ΔarcD**	**P value**	**Pm + Ef**	**ΔargF + ΔarcD**	**P value**
Bladder hematoma and/or blood in urine	1/13	0/11	0.306	0/20	0/18	>0.999	0/14	0/13	>0.999
Kidney hematoma	3/13	0/11	0.088	0/20	0/18	>0.999	5/14	0/13	0.011*
Kidney color change and/or mottling	1/13	0/11	0.347	0/20	0/18	>0.999	8/14	2/13	0.013*
Kidney stone	2/13	3/11	0.475	0/20	0/18	>0.999	5/14	1/13	0.054
Any abnormality	4/13	3/11	0.099	0/20	0/18	>0.999	8/14	2/13	0.013*
Bacteremia	11/13	4/11	0.015*	0/20	0/18	>0.999	13/14	6/13	0.003*

Figure Legends

Figure 1. *P. mirabilis* and *E. faecalis* polymicrobial biofilms exhibit enhanced biofilm biomass that is driven by biofilm compositional changes and not bacterial counts. A) Crystal violet staining of biofilms grown for 24hrs in TSB-G. B) Colony forming units of biofilms grown for 24hrs in TSB-G. Data represent the mean ± standard deviation for 3-5 independent experiments with at least three replicates each. ns = non-significant, One-way ANOVA multiple comparisons, * $p<0.05$, *** $p<0.001$, **** $p<0.0001$. Biofilm compositional analysis of 20-hour single or polymicrobial biofilms detailing C) total eDNA, d) total carbohydrate, E) total protein, and F) proteinase-K treatment of polymicrobial biofilm abrogates the enhancement phenotype. BS = biofilm supernatant fraction, CF = cell associated fraction, EPS = extrapolymeric substance fraction. Data represent the mean ± standard deviation for at least three independent experiments with at least two replicates each. ns = non-significant, * $p<0.05$, ** $p<0.01$, *** $p<0.001$, **** $p<0.0001$ by repeated measures one-way ANOVA.

Figure 2. Schematic of *P. mirabilis* L-ornithine and L-arginine metabolism. All known genes involved in L-ornithine metabolism and L-arginine biosynthesis in *P. mirabilis* are displayed. L-ornithine can either be directly catabolized to putrescine via ornithine decarboxylate (SpeF), or it can feed into L-arginine biosynthesis via ornithine carbamoyltransferse (ArgF), which generates L-citrulline. Argininosuccinate synthase (PMI_RS16015) uses ATP to generate L-arginino-succinate from L-citrulline and L-aspartate, then argininosuccinate lyase (ArgH) generates L-

arginine and fumarate from L-arginino-succinate. L-arginine can then be catabolized to putrescine via arginine decarboxylase (SpeA) and agmatinase (SpeB).

Figure 3. Ornithine and arginine metabolism are key determinants of *P. mirabilis* growth *in vitro* in both laboratory media and physiologically relevant pooled human urine. *Enterococcus faecalis* growth curves in A) BHI, B) TSB-G, and C) pooled human urine. *Proteus mirabilis* growth curves in D) TSB-G E) low-salt LB, F) PMSM (*Proteus* minimal salts media), G) PMSM supplemented with 10 mM supplemented ornithine, H) PMSM supplemented with 10mM arginine, I) PMSM supplemented with 10 mM citrulline, and J) pooled human urine. Data represent the mean and standard deviation of at least three biological replicates.

Figure 4. L-ornithine secretion from *E. faecalis* and arginine biosynthesis by *P. mirabilis* are critical drivers of increased biofilm biomass production. Crystal violet staining of biofilms grown for 24hrs in TSB-G with either A) no supplementation, B) 10 mM ornithine, C) 10 mM arginine, D) or 10mM agmatine. E) Total protein of pooled biofilm fractions of polymicrobial biofilms grown for 24-hours in TSB-G. F) Crystal violet staining of biofilms grown for 24-hours in pooled human urine. Data represent the mean ± standard deviation for 3-5 independent experiments with at least two replicates each. ns = non-significant, One-way ANOVA multiple comparisons, *$p<0.05$, ***$p<0.001$, ****$p<0.0001$.

Figure 5. Disruption of metabolic cooperation between *E. faecalis* and *P. mirabilis* decreases dissemination of polymicrobial CAUTI infection. Bacterial counts in urine (U),

bladder (B), kidneys (K), and spleens (S) samples collected at 96hrs post infection in CAUTI murine model. Single-species infections were conducted with 10^5 CFUs/mL of either A) wild type *P. mirabilis* or *P. mirabilis* Δ*argF*, or B) wild type *E. faecalis* or *E. faecalis* Δ*arcD.* C) Polymicrobial infections were conducted with 50:50 mixtures of both wild-type species or both mutants, and each datapoint represents the total bacterial burden per organ. *$p<0.05$ by nonparametric One-Way ANOVA.

Supplement 1. Characterization of *P. mirabilis* virulence factors in the metabolic mutants shows no changes in other common virulence phenotypes. A) Urease activity was measured via urease activity phenol red assay. Absorbance OD_{562} was measured at every minute for 120 minutes. Urease activity was expressed as the area under the curve of mean change in optical density per minute. *P. mirabilis* urease deficient mutant, *ureF*, was used as a negative control. B) Swimming motility of each strain was determined after incubation overnight at 30°C and reported as the diameter of the swimming ring. C) Swarming motility of each strain was measured after incubation overnight at 37°C. The diameter of each swarming ring was measured and reported. Data is representative of three biological replicate experiments.

Supplement 2. Growth of *argF* is not restored by supplementation with agmatine or putrescine. PMSM growth curves supplemented with A) 10mM agmatine or B) 10 mM putrescine. Data is representative of three biological replicate experiments.

Supplemental 3. Fitness of *P. mirabilis argF*, *P. mirabilis speF*, and *E. faecalis arcD* during growth in human urine. Competitive index (CI) of co-inoculated A) wild-type *P. mirabilis* and *speF* mutant in pooled human urine, B) wild-type *P. mirabilis* and *argF* mutant in pooled human urine, C) wild-type *P. mirabilis* and *argF* mutant in pooled human urine with 10 mM citrulline supplementation, or D) wild-type *E. faecalis* and *arcD* mutant in pooled human urine. Each symbol represents the $\log_{10}$ CI for an individual inoculum, error bars represent the medians and dashed line indicates the $\log_{10}$ CI = 0 (the expected value if the ratio of mutant/WT is 1:1). E) *P. mirabilis* and *argF* CFUs over the time course used to calculate the CI. F) *E. faecalis* and *arcD*

CFUs over the time course used to calculate the CI. Error bars represent mean and standard deviation. *P<0.05, **P<0.01 by two-way ANOVA comparison to wild-type CFUs.

Supplemental figure 4. Changes in colony forming units between wild-type and mutant biofilms is insignificant and not a driving factor for the differences in biofilm biomass. CFUs of biofilms grown for 24-hours in A) TSB-G or B) pooled human urine. Data represent the mean ± standard deviation for at least three independent experiments with at least two replicates each. ns = non-significant, * = P<.05 as determined by One-way ANOVA.

Supplemental 5. Colony forming units of each species from coinfected mice. *P. mirabilis* and *E. faecalis* bacterial counts in urine (U), bladder (B), kidney (K), and spleen (S) homogenates from an individual coinfected mouse are connected with a black line.

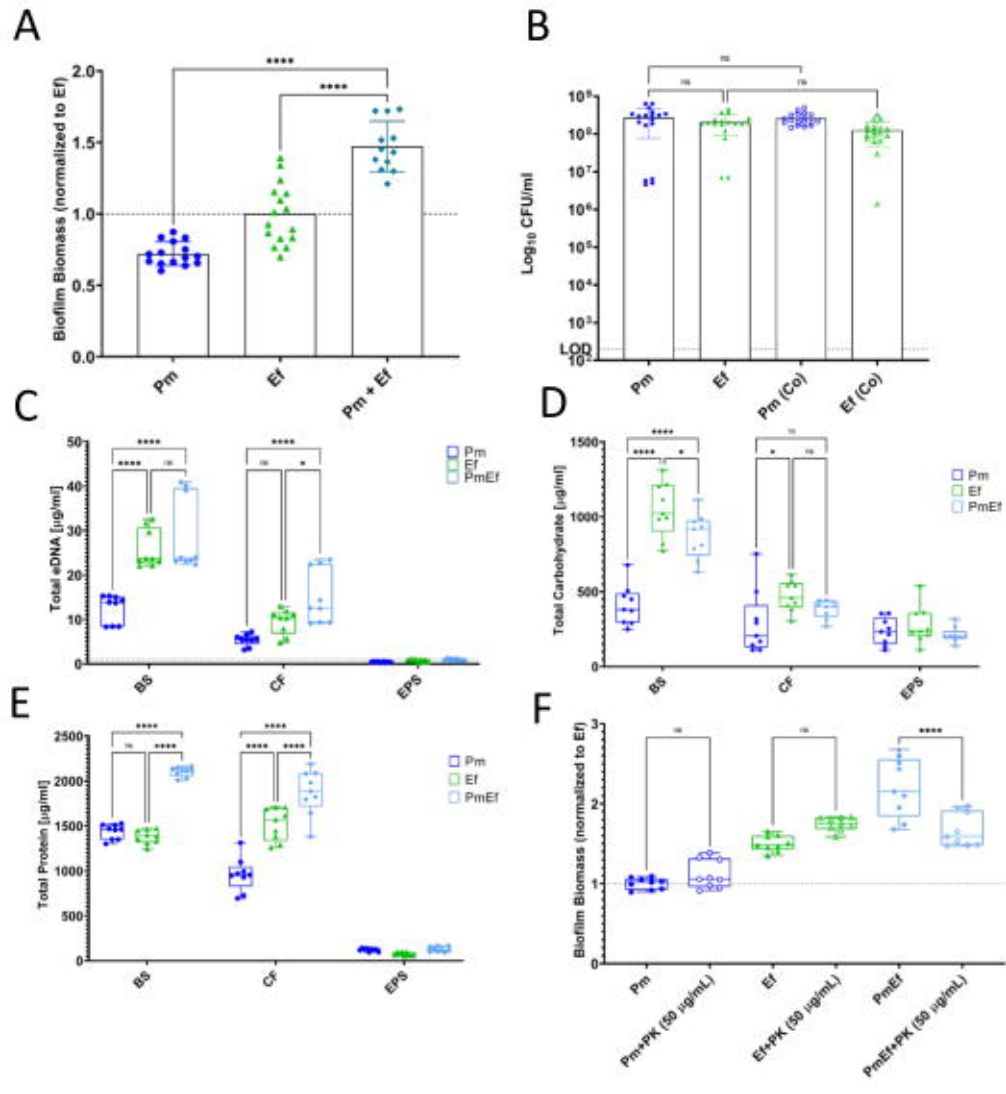
A
Biofilm Biomass (normalized to Ef)
2.0
1.5
1.0
0.5
0.0
****
****
Pm
Ef
Pm + Ef
B
Log10 CFU/ml
LOD
ns
ns
ns
Pm
Ef
Pm (Co)
Ef (Co)
C
Total eDNA [µg/ml]
Pm
Ef
PmEf
BS
CF
EPS
D
Total Carbohydrate [µg/ml]
Pm
Ef
PmEf
BS
CF
EPS
E
Total Protein [µg/ml]
Pm
Ef
PmEf
BS
CF
EPS
F
Biofilm Biomass (normalized to Ef)
Pm
Pm+PK (50 µg/mL)
Ef
Ef+PK (50 µg/mL)
PmEf
PmEf+PK (50 µg/mL)

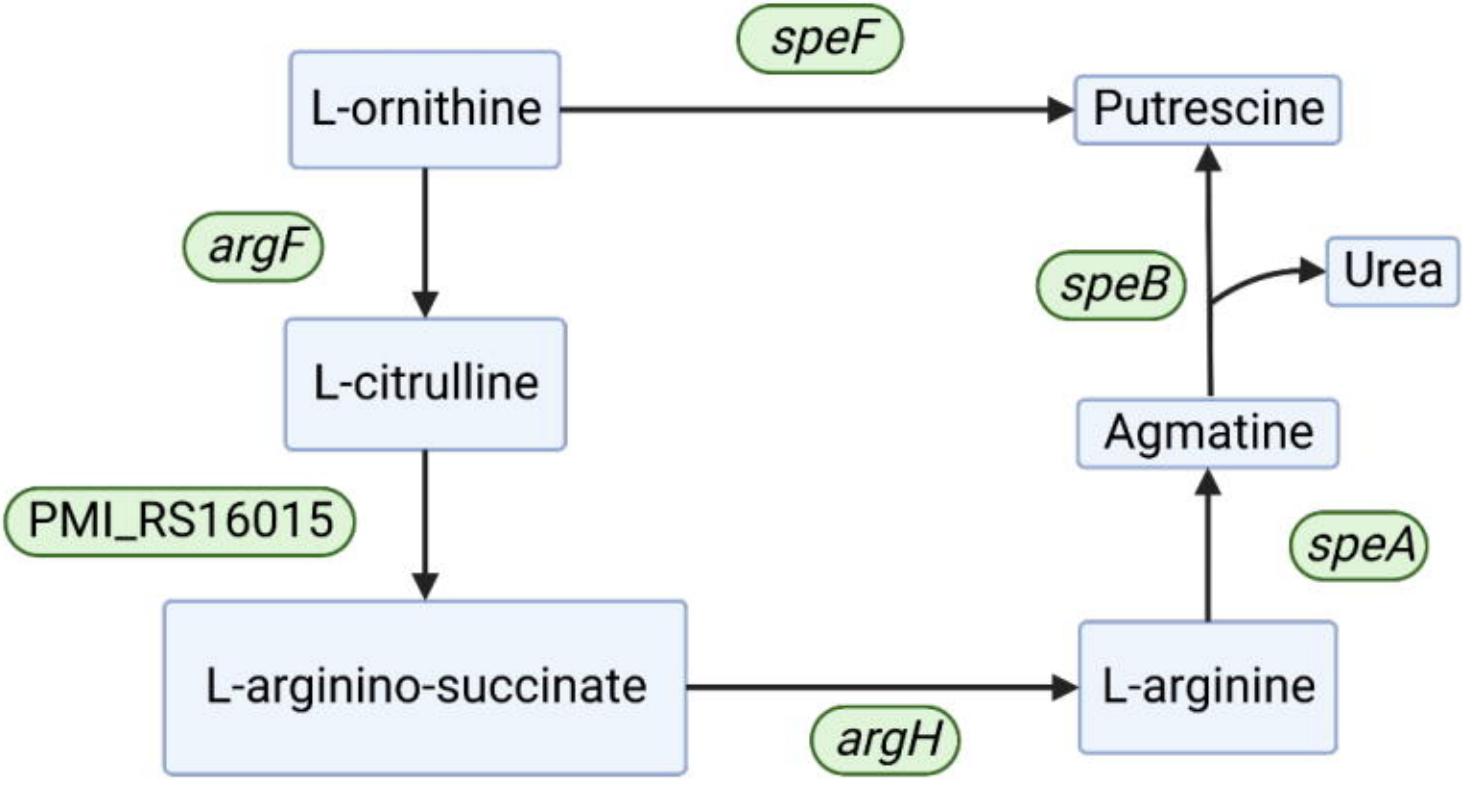
speF
L-ornithine
Putrescine
argF
speB
Urea
L-citrulline
Agmatine
PMI_RS16015
speA
L-arginino-succinate
L-arginine
argH

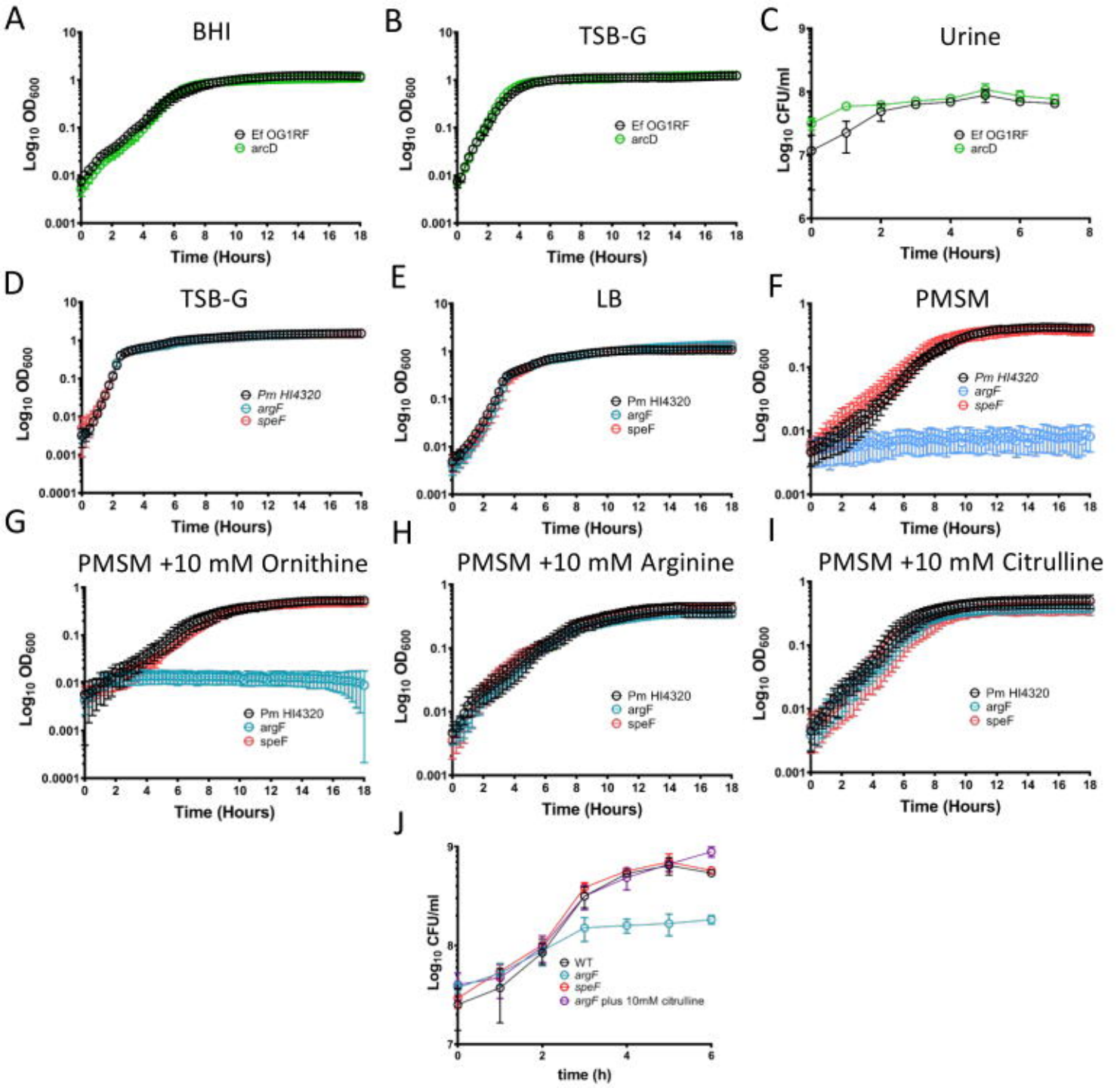
A
BHI
Log10 OD600
Time (Hours)
Ef OG1RF
arcD
B
TSB-G
Log10 OD600
Time (Hours)
Ef OG1RF
arcD
C
Urine
Log10 CFU/ml
Time (Hours)
Ef OG1RF
arcD
D
TSB-G
Log10 OD600
Time (Hours)
Pm HI4320
argF
speF
E
LB
Log10 OD600
Time (Hours)
Pm HI4320
argF
speF
F
PMSM
Log10 OD600
Time (Hours)
Pm HI4320
argF
speF
G
PMSM +10 mM Ornithine
Log10 OD600
Time (Hours)
Pm HI4320
argF
speF
H
PMSM +10 mM Arginine
Log10 OD600
Time (Hours)
Pm HI4320
argF
speF
I
PMSM +10 mM Citrulline
Log10 OD600
Time (Hours)
Pm HI4320
argF
speF
J
Log10 CFU/ml
time (h)
WT
argF
speF
argF plus 10mM citrulline

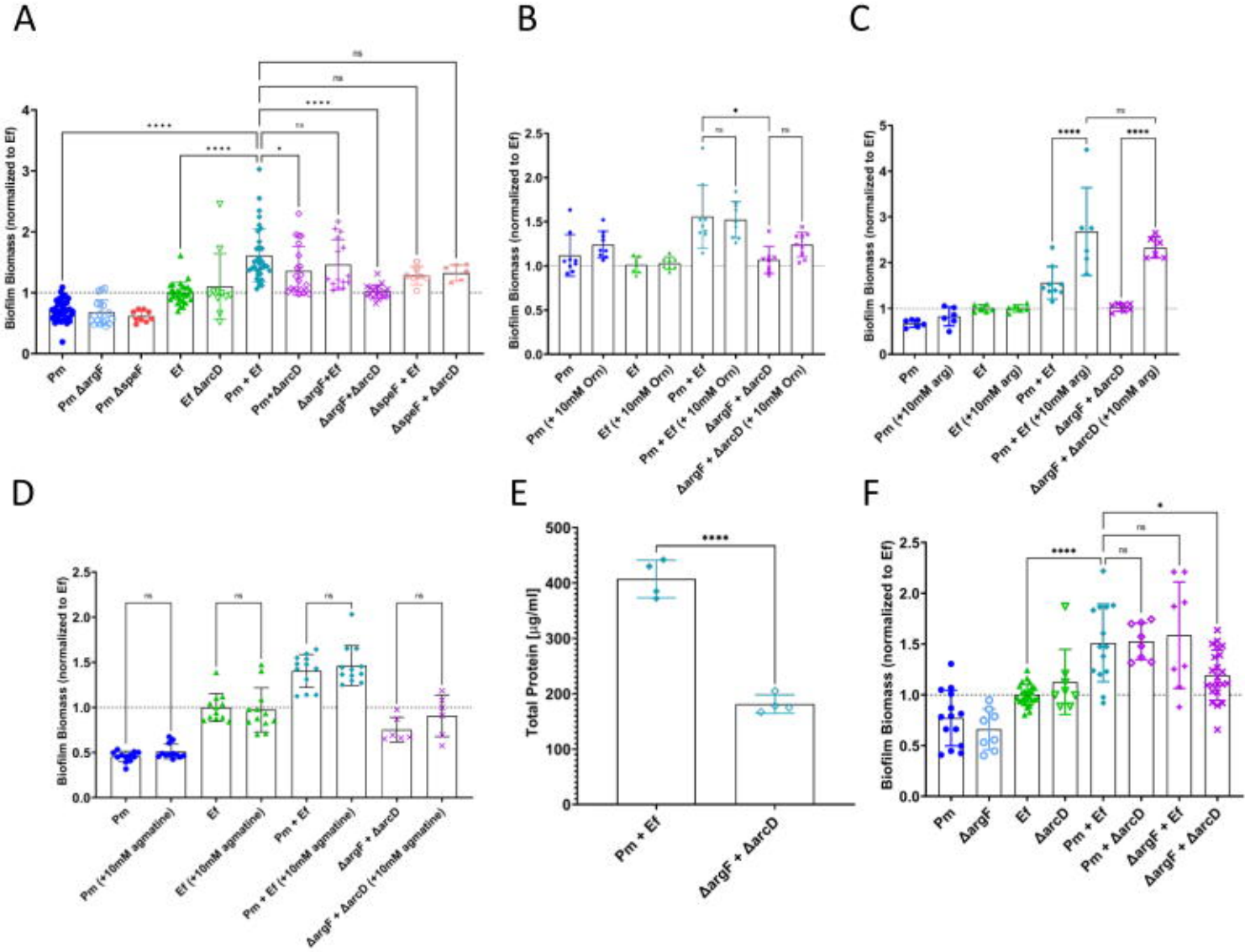
A
Biofilm Biomass (normalized to Ef)
Pm
Pm ΔargF
Pm ΔspeF
Ef
Ef ΔarcD
Pm + Ef
Pm+ΔarcD
ΔargF+Ef
ΔargF+ΔarcD
ΔspeF + Ef
ΔspeF + ΔarcD
B
Biofilm Biomass (normalized to Ef)
Pm
Pm (+ 10mM Orn)
Ef
Ef (+ 10mM Orn)
Pm + Ef
Pm + Ef (+ 10mM Orn)
ΔargF + ΔarcD
ΔargF + ΔarcD (+ 10mM Orn)
C
Biofilm Biomass (normalized to Ef)
Pm
Pm (+10mM arg)
Ef
Ef (+10mM arg)
Pm + Ef
Pm + Ef (+10mM arg)
ΔargF + ΔarcD
ΔargF + ΔarcD (+10mM arg)
D
Biofilm Biomass (normalized to Ef)
Pm
Pm (+10mM agmatine)
Ef
Ef (+10mM agmatine)
Pm + Ef
Pm + Ef (+10mM agmatine)
ΔargF + ΔarcD
ΔargF + ΔarcD (+10mM agmatine)
E
Total Protein [µg/ml]
Pm + Ef
ΔargF + ΔarcD
F
Biofilm Biomass (normalized to Ef)
Pm
ΔargF
Ef
ΔarcD
Pm + Ef
Pm + ΔarcD
ΔargF + Ef
ΔargF + ΔarcD

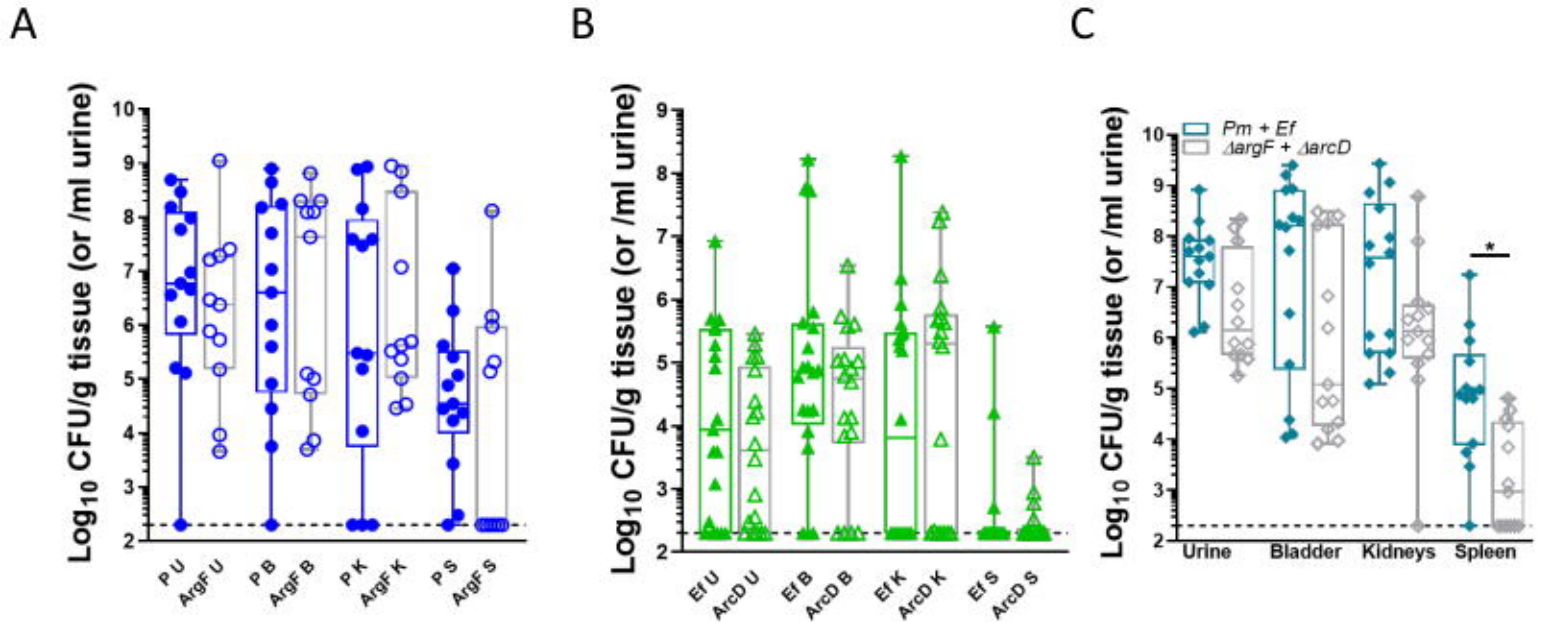
A
B
C
Log10 CFU/g tissue (or /ml urine)
P U
ArgF U
P B
ArgF B
P K
ArgF K
P S
ArgF S
Ef U
ArcD U
Ef B
ArcD B
Ef K
ArcD K
Ef S
ArcD S
Pm + Ef
ΔargF + ΔarcD
*
Urine
Bladder
Kidneys
Spleen